Yuan *et al. Microstructures* **2025**, *5*, 2025053
DOI: 10.20517/microstructures.2024.100

Microstructures

Research Article

Open Access

Check for updates

High-throughput screening of superlattice-like Ge-Sb-M (M = Sn, Se) thin films for multi-level phase change photonics materials

Hongjian Yuan[1,2], Junyuan Lu[1], Genmao Zhuang[1], Hong Wang[1,2,3], Jian Hui[1,2,3]

[1]School of Materials Science and Engineering, Shanghai Jiao Tong University, Shanghai 200240, China.
[2]Zhangjiang Institute for Advanced Study, Shanghai Jiao Tong University, Shanghai 201210, China.
[3]Suzhou Laboratory, Suzhou 215000, Jiangsu, China.

Correspondence to: Dr. Jian Hui, School of Materials Science and Engineering, Shanghai Jiao Tong University, Shanghai 200240, China; Zhangjiang Institute for Advanced Study, Shanghai Jiao Tong University, Shanghai 201210, China. E-mail: hj20151107@sjtu.edu.cn

How to cite this article: Yuan, H.; Lu, J.; Zhuang, G.; Wang, H.; Hui, J. High-throughput screening of superlattice-like Ge-Sb-M (M = Sn, Se) thin films for multi-level phase change photonics materials. *Microstructures* **2025**, *5*, 2025053. https://dx.doi.org/10. 20517/microstructures.2024.100

Received: 17 Oct 2024 **First Decision:** 26 Nov 2024 **Revised:** 20 Dec 2024 **Accepted:** 31 Dec 2024 **Published:** 22 Apr 2025

Academic Editor: Zhihua Sun **Copy Editor:** Fangling Lan **Production Editor:** Fangling Lan

Abstract

Ge-Sb-Sn/Se with a superlattice-like structure (SLL) is a promising material candidate for multi-level phase change photonics memory technology. However, its multi-stage phase transition process has not been elucidated so far due to the limitations of traditional research approaches. The most critical issue is to efficiently construct its composition-process-structure-property multi-parameter coupled constitutive relationship. In this work, we develop a high-throughput approach to systematically study the multi-level phase transition mechanisms of Ge-Sb-Sn/Se SLL combinatorial thin films. For the Ge-Sb-Sn system, phase evolution is observed from trigonal to hexagonal/tetrahedral structures. In contrast, the Ge-Sb-Se system behaves differently. We further examine the optical properties of the Ge-Sb-Sn/Se SLL combinatorial thin films. The results identify the $GeSbSn_3$ SLL thin film as a standout from the Ge-Sb-Sn ternary system under Sb→Sn→Ge deposition sequence, with a figure of merit (FOM) greater than 0.4 and high thermal stability. The present study serves as a foundation for further exploration of the Ge-Sb-based quaternary system and accelerates the application of advanced phase change materials (PCMs) in the big data era.

Keywords: Ge-Sb-Se/Sn, superlattice-like thin film, high-throughput, multi-level phase transition, optical properties

INTRODUCTION

In the era of rapid advances in artificial intelligence and distributed computing, data generation has reached unprecedented levels. To meet the growing demand for data storage, non-volatile memory technologies with multi-level storage capabilities are emerging, which offer great potential to break the physical limitations of traditional computer memory architectures[1,2]. Chalcogenide phase change materials (CPCMs), particularly $Ge_2Sb_2Te_5$ (GST) as a representative example, have emerged as promising candidates for multi-level storage[3,4]. GST displays a distinctive crystallization evolution process, transitioning from an amorphous state to a face-centered cubic (FCC) structure and subsequently to a hexagonal (HEX) structure[5]. The pronounced contrasts in electrical and optical properties between its amorphous and crystalline states enable advanced data storage solutions[6].

However, high power consumption remains a major barrier to the widespread deployment of conventional CPCMs. Extensive studies have explored the influence of various dopants on Ge-Sb-Te chalcogenide thin films, including metallic[7,8], semiconductor[9,10], and specific non-metallic elements[11,12]. Within the studies, two prominent approaches have been proposed to decrease the energy consumption of CPCMs for applications on all-photonic spiking neural networks. The first approach focuses on reducing the power required for the phase change between amorphous and crystalline states through heat treatment or an electric current[13]. Notably, the energy consumption associated with the phase change from the crystalline to the amorphous state (often referred to as the RESET operation) is typically higher, particularly during repeated cycling in practical applications[14]. Doping Sn in GST[15,16] is a commonly effective strategy to lower the bond dissociation energy and the melting point of the system, thereby lowering the energy barrier for the RESET operation. The second approach is to enhance the non-volatile optical switching contrast and reduce the optical loss upon phase transition[17], which is essential for waveguide fabrication in integrated optics[18,19]. Replacing heavier Te atoms with Se has been shown to reduce lattice phonon energies, broadening transparency in the mid-infrared region[20]. Notably, the development of a novel CPCM ($Ge_2Sb_2Se_4Te_1$) has achieved an unprecedented optical figure of merit (*FOM*)[21], indicating significantly lower optical loss and higher optical switching contrast compared to conventional GST alloys.

Reducing power consumption during the phase transition between the amorphous and crystalline states often compromises the stability of the amorphous phase[14]. Introducing a superlattice-like structure (SLL) in CPCMs has emerged as a promising approach to realizing multi-level memory with a balance of low power consumption and good amorphous stability. This approach increases the phonon scattering at the interfaces and modifies unique electronic structures controlling the phase transition process[22,23]. Nevertheless, the characteristics of SLL structure can be altered by subtle variations in period, synthesis conditions, *etc*. A comprehensive understanding of the structural evolutions of Ge-Sb-Sn and Ge-Sb-Se SLL thin films remains lacking, impeding their further applications in multi-level data memories.

In this work, we propose an approach that integrates combinatorial synthesis, high-throughput characterization, and machine learning methods to accelerate the discovery of promising multi-level phase change photonics materials in the Ge-Sb-Sn and Ge-Sb-Se ternary systems. High-throughput ion beam deposition was employed to synthesize Ge-Sb-Sn and Ge-Sb-Se thin films with a SLL structure. High-throughput X-ray diffraction (XRD) and ellipsometry were systematically performed on the combinatorial Ge-Sb-Sn and Ge-Sb-Se SLL thin films as a function of deposition sequence and temperature across the entire ternary compositional space. Through this process, we identified several novel CPCMs with improved amorphous stability and superior optical performance for potential application in multi-level photonic memories. Meanwhile, we established a comprehensive AI-ready experimental database for Ge-Sb-Sn and Ge-Sb-Se SLL thin films, which supports our ongoing work in constructing an active learning-

assisted workflow for the rapid discovery of optical CPCMs.

MATERIALS AND METHODS

SLL thin-film synthesis with a combinatorial method

Combinatorial SLL thin films of the Ge-Sb-Sn and Ge-Sb-Se ternary systems were synthesized at room temperature with a high-throughput ion beam deposition system, as illustrated in Figure 1. A more detailed view of the morphology of the combinatorial SLL thin film can be found in Supplementary Figure 1. Prior studies have revealed that the coating sequence of chalcogens (such as Se) in a modulation period has a significant effect on the multilayer SLL structure[23]. The chalcogen layer initially mixes with Ge before Sb arrives, leading to the subsequent reactions between the mixed layer and adjacent Sb. Therefore, in this work, Ge and Sb were chosen as the initial layer. The deposition sequences were designed as Ge→Sb→Sn (GSSn-1), Sb→Sn→Ge (GSSn-2), Ge→Sb→Se (GSSe-1), and Sb→Se→Ge (GSSe-2) with a modulation period of 20 nm. The side length of the combinatorial thin films was 21.6 mm. A 3-nm-thick capping layer of Si_3N_4 was deposited on the surface of the thin films to prevent oxidation. The as-deposited thin films were isothermally annealed in a turbopump vacuum furnace with a vacuum of 10^{-4} torr for one hour at 473 and 573 K, respectively. These annealing temperatures were selected based on the phase transition temperature range of the Ge-Sb-based ternary systems, which typically spans from 423 K to around 623 K[24-26]. More details of the synthetic method are described in our previous work[27].

High-throughput chemical composition analysis

An M4 TORNADO micro-X-ray Fluorescence (XRF) spectrometer (Bruker, Germany) was used to calibrate the chemical composition of the thin films with a step size of 150 um. The intensity signals of each element were calibrated and converted into thickness values through the M4 TORNADO XMETHOD application (Bruker GmbH, Germany).

High-throughput structure analysis of the combinatorial thin films

We developed coordinate conversion software to ensure spatial coordinate consistency and automate the generation of scan test paths for different high-throughput characterization systems. Structure information was acquired on a Bruker D8 Discovery diffractometer using Cu $K\alpha_1$ (λ = 1.5406 Å) at room temperature. The intensity data were collected by a 2D-detector over a 2θ range of 10° to 60°. A motorized mobile X-Y-Z stage that holds samples allows the measurement of the entire thin film with a step size of 1 mm, controlled by an easy and automatic algorithm. In this study, triangular scan paths were designed to characterize 210 data points on each sample.

High throughput XRD experimental data collected by the 2D detector was initially transformed into 1D data, following the procedure outlined in our prior study[28]. Subsequently, we employed an unsupervised machine learning-based workflow for exploratory data analysis and phase mapping. To identify the characteristic peaks, the "pybaselines" package[29] and Gaussian filtering were preliminarily employed to eliminate noise and substrate signals. The built-in functions of "scipy.signal" package[30] were used to find the diffraction peaks based on the defined threshold of peak height and peak width. The peak locations taken from the spectra served as a Boolean vector r_i as follows:

$$r_i = (w_1, w_2, \cdots, w_k) \tag{1}$$

where w_k is 1 if a peak exists at the w-th position and otherwise 0.

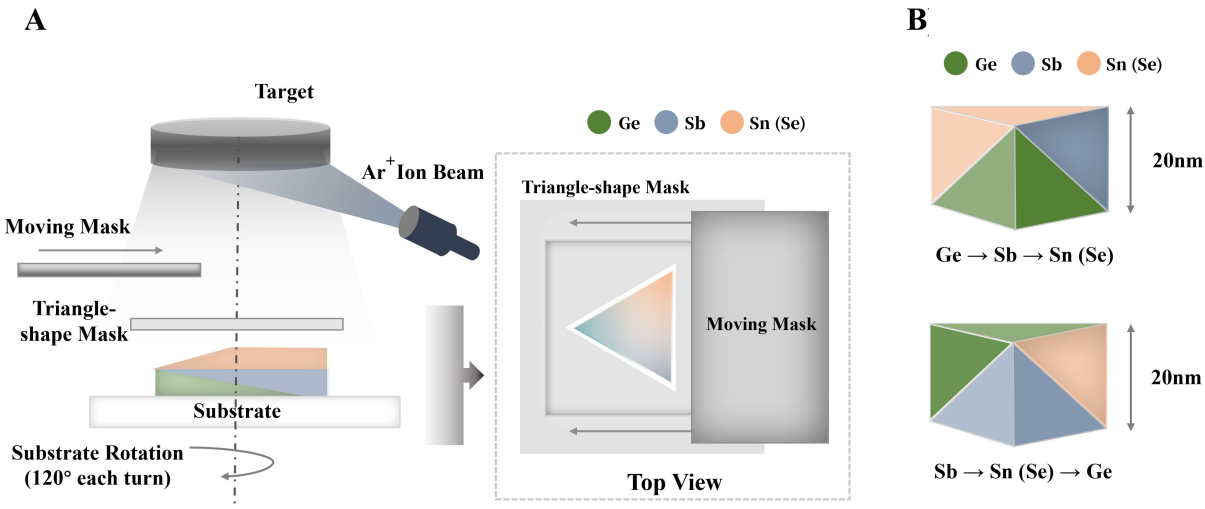

Figure 1. Schematics diagram of Ge-Sb-Sn and Ge-Sb-Se combinatorial SLL thin films. (A) High-throughput deposition process using a movable mask (for generating gradient component distribution) and a triangle-shape mask; (B) Cross section of the thin films with distinct coating sequences (Ge→Sb→Sn/Se and Sb→Sn/Se→Ge).

The specific phases were automatically identified using the hierarchical clustering method[31], which grouped the Boolean vectors and segmented them into separate clusters based on a predefined threshold for peak shift. If a peak position of a Boolean vector exceeds the predefined threshold, the clustering method will identify it as a new cluster. Subsequently, the corresponding phases of each cluster were determined by referencing the Inorganic Crystal Structure Database (ICSD). Several clusters may be merged into a single cluster based on the query results of the ICSD.

High-hroughput optical measurement and analysis

Spectroscopic ellipsometry measurements were conducted on combinatorial SLL thin films using an RC2 Woollam Vertical-Variable Angle Spectroscopic Ellipsometer (J. A. Woollam Co., Lincoln, NE, USA). The measurements were taken at angles of incidence (AOI) of 50°, 60°, and 70°, covering a spectral range from 500 to 2,100 nm. On each combinatorial SLL thin film, 630 data points were characterized along a triangular scan path with a step size of 620 μm.

A self-developed three-layer model was constructed using *CompleteEase* software (J. A. Woollam Co., Lincoln, NE, USA), containing: (1) A SiO_2 Sellmeier dispersion model for the substrate at the bottom; (2) a 20 nm B-spline model for the Ge-Sb-Sn and Ge-Sb-Se SLL thin films at the middle layer; (3) a 3 nm TaucLorentz oscillator model for the Si_3N_4 capping layer at the top. The refractive index (n) and extinction coefficient (k) of the Ge-Sb-Sn and Ge-Sb-Se SLL thin films were determined by the B-Spline model. The fitting was performed as a function of wavelength and angle of incidence. The B-spline model is unaffected by factors including the structure of materials and varied absorption characteristics at various wavelengths[32]. Thus, it is suitable for automated high-throughput analysis in multilayer thin films. The Kramers-Kronig (K-K) relation between the dielectric constants was maintained throughout the fitting process, and the dielectric constant ε_2 was set to no less than 0, ensuring the physical consistency of the fitting results.

RESULTS AND DISCUSSION

The compositions of the SLL thin films were in perfect agreement with our experimental design, as shown in Supplementary Figure 2. The effects of the composition and coating sequence on the structural

evolutions and the optical performance of Ge-Sb-Sn and Ge-Sb-Se SLL thin films were thoroughly investigated based on high-throughput characterization and data analysis described in the Section "METHODS".

Structural evolution of SLL thin films

Ge-Sb-Sn ternary system

The phase diagrams of GSSn-1 and GSSn-2 are shown in Figure 2. Under both coating sequences, the as-deposited thin films were predominantly amorphous across the entire composition range, except for a few instances near the Sn-rich region, as shown in Supplementary Figure 3. The phase diagrams of the GSSn-1 and GSSn-2 SLL thin films consist of two single-element phases (Sn, ICSD no.106072 and Sb, ICSD no.161493) and five solid-solution phases, which shared the same structure of ICSD no.126294, ICSD no.651573, ICSD no.52226, ICSD no.43216, and ICSD no.112680, respectively. Representative XRD patterns of the SLL thin films can be found in Supplementary Figures 4-6.

The effect of temperature on phase evolution was studied by comparison of the phase distribution of GSSn-1 and GSSn-2 SLL thin films annealed at 473 and 573 K. The following observations were made from the GSSn-1 phase distribution maps:

(1) In general, the amorphous region reduces as the temperature increases, a trend that also applies to GSSn-2 and Ge-Sb-Se SLL thin films.

(2) With the increase in Sn component at 473 K, the SbSn solid solution transformed from trigonal (R-3m) to tetragonal (I41/amdS) structure, which is consistent with the stable phase of the two single-element phases. Since Sb and Sn have similar atomic radii (Sb: 133 pm, Sn: 145 pm), the substitution of the two elements in the sublattice structure generally does not require overcoming a large energy barrier. This substitution effect is frequently discovered between Sb and Ge[33], as well as between Sb and many of the chalcogens[34].

(3) As the annealing temperature increased from 473 to 573 K, the hexagonal (P63/mmc) structure appeared and coexisted with the original trigonal (R-3m) phase at the Sb-rich corner, which turned out to be the more stable phase at a higher temperature. Similar results have been observed in pure Sb[35]. Furthermore, our observations suggest a phase transition from a tetragonal (I4/amdS) to a tetragonal (I4/mmm) structure near the Sn-rich corner at 573 K in GSSn-1 SLL thin films. Notably, the I4/mmm space group structure closely resembles the one reported at 10.8 GPa[36], with minor variations in lattice parameters attributed to the elevated pressure conditions.

(4) In a small area near the midpoint of the SbSn-GeSn compositional line, crystallization signals disappeared after the increase in annealing temperature. This phenomenon can be attributed to the enhanced mobility of Ge atoms at elevated temperatures, which promotes the diffusion and aggregation of Sn atoms, ultimately destabilizing the tetragonal lattice structure[37].

Changing the deposition sequence from GSSn-1 to GSSn-2 improved the amorphous stability of the Ge-Sb-Sn-SLL thin films. From the GSSn-2 phase distribution maps shown in Figure 2, the formation of tetragonal (I41/amdS and I4/mmm) phases was suppressed. The majority of the solid solution remained in the R-3m space group, while only a small portion of the data at the Sb-rich corner contained a crystalline signal of hexagonal (P63/mmc) phase structure. The observed suppression originates from competing crystallization pathways between the R-3m and I4/amdS structures in SbSn, mediated through Ge amorphization toward

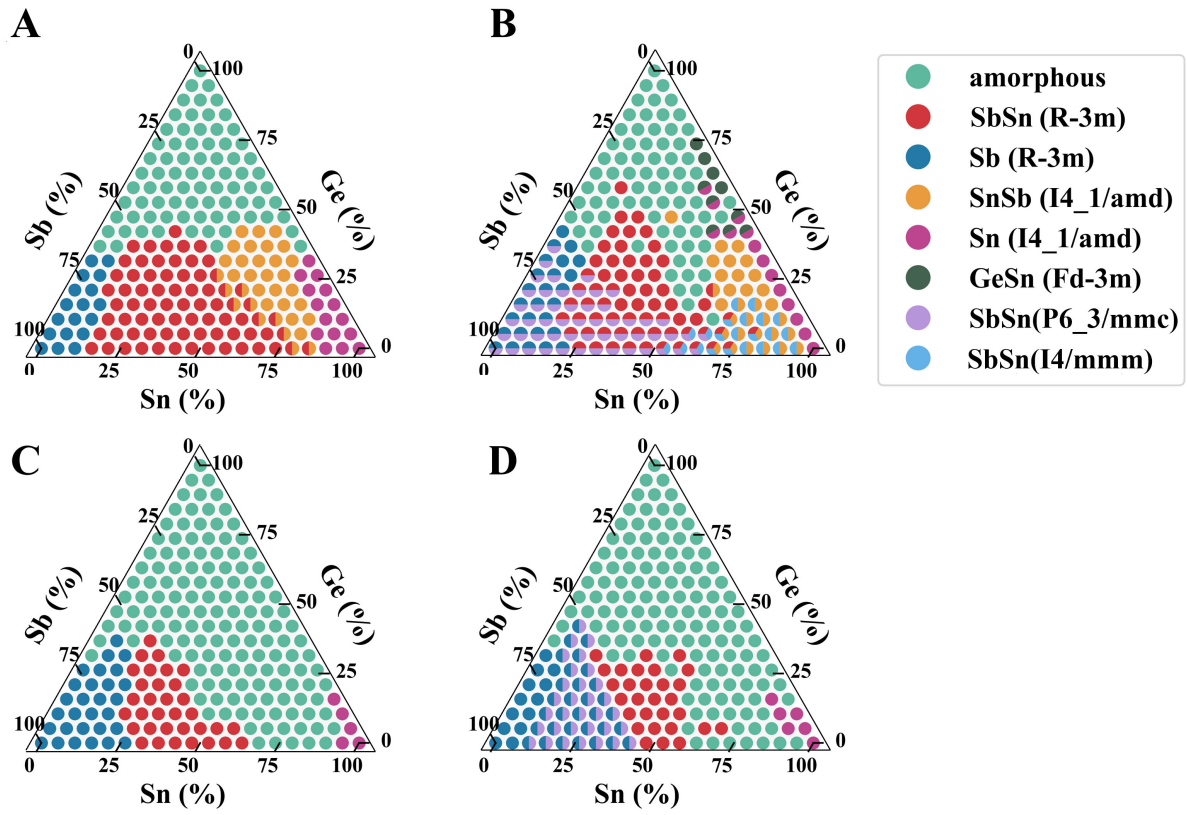

Figure 2. Phase distribution map of Ge-Sb-Sn SLL thin films. (A) GSSn-1 after annealed at 423 K for 1 h; (B) GSSn-1 after annealed at 573 K for 1 h; (C) GSSn-2 after annealed at 423 K for 1 h; (D) GSSn-2 after annealed at 573 K for 1 h.

the Sb-M (M = Sn, Se) epitaxial layer. In the Ge→Sb→M deposition sequence, amorphous Ge serves as the underlying layer in a modulation period, suppressing the crystallization tendency of Sb towards the R-3m structure during subsequent annealing[38]. Therefore, the I4/amdS space group is more likely to form in regions with higher Sn concentrations. Several studies have also observed substrate-induced phase-mediated behavior, emphasizing its importance in microstructure control[39,40].

In both coating sequences, a continuous transition process from Sb (R-3m) to SbSn (R-3m) was noted, which can be proved by Supplementary Figure 7. The gradient doping of Sn resulted in a continuous shift of the main peak around 29° (1 0 1) due to lattice distortion induced by the substitution effect. Consistent with the experimental results in ICSD, the peak position shifted to a higher angle with increasing Sn content. The lattice spacing distribution of the (1 0 1) orientation of GSSn-1 SLL thin film at 573 K ranged from 1.5753 ± 0.0039 to 1.5992 ± 0.0039 Å. Furthermore, with the transition from Sb (R-3m) to SbSn (R-3m), the preferential orientation of the R-3m space group in the SLL thin films also changed from (0 1 -4) and (0 0 6) to (2 -1 0) [Supplementary Figure 8]. Peaks in the predominant texture orientation of the thin films exhibit the highest intensity and generally indicate the most stable state, while others are either weakly expressed or completely absent.

Ge-Sb-Se ternary system

The phase diagrams of GSSe-1 and GSSe-2 are shown in Figure 3. Under both coating sequences, the as-deposited thin films were predominantly amorphous across the entire composition range, except for a few crystalline regions near the Sb-rich side. Se-based alloys have higher crystallization temperatures and lower

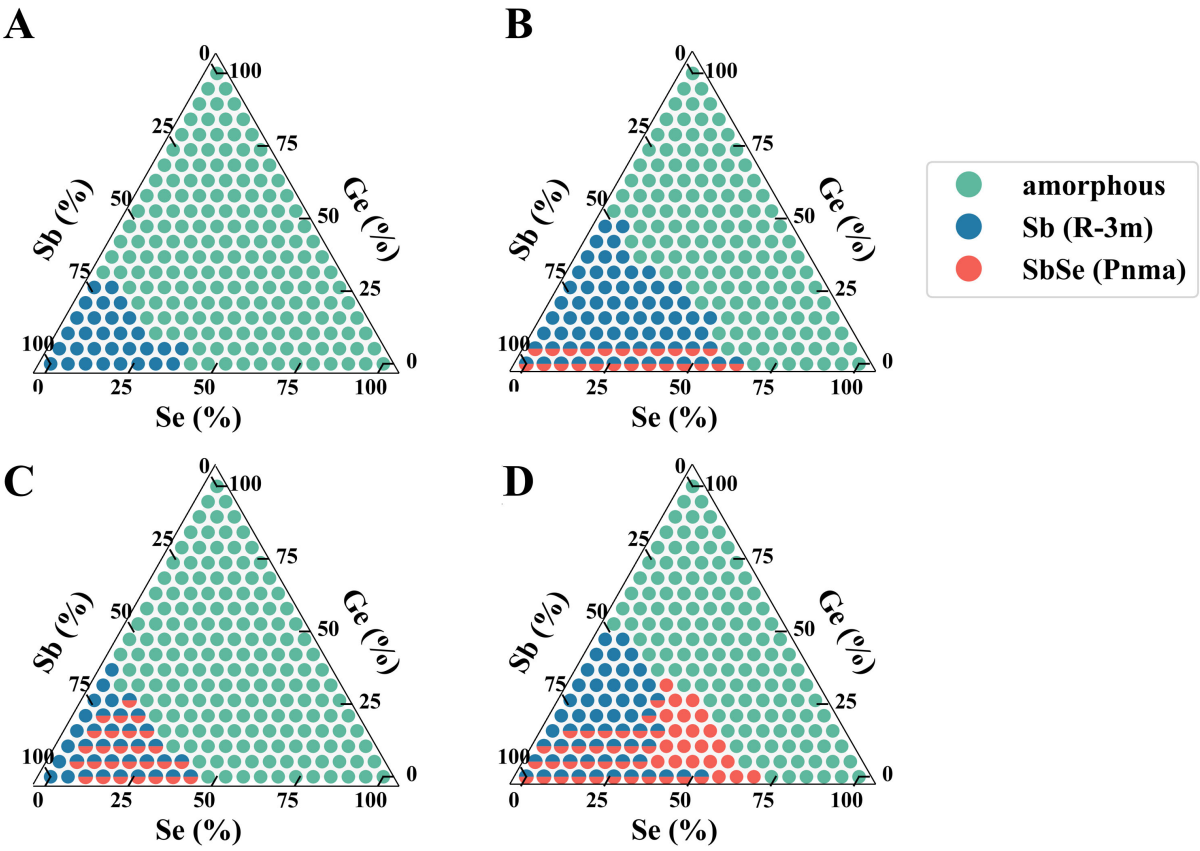

Figure 3. Phase distribution map of Ge-Sb-Se SLL thin films. (A) GSSe-1 after annealed at 423 K for 1 h; (B) GSSe-1 after annealed at 573 K for 1 h; (C) GSSe-2 after annealed at 423 K for 1 h; (D) GSSe-2 after annealed at 573 K for 1 h.

melting points than GST225. Moreover, a reduction in Ge content further enhances the thermal stability of the amorphous state. Thus, no Se single-element phase was observed at temperatures up to 573 K. The phase diagrams of the GSSe-1 and GSSe-2 libraries consist of a single-element phase (Sb) and a region of solid solution (Sb_2Se_3, ICSD no.194836).

Both GSSe-1 and GSSe-2 coating sequences show a similar phase transition process. Under the annealing temperature of 473 K for GSSe-1, only trigonal (R-3m) signals existed at the Sb-rich corner. As the annealing temperature increased from 473 to 573 K, the orthorhombic (Pnma) phase occurred at the Se-rich side with a low content of Ge, which turned out to be the more stable phase at a higher temperature. For GSSe-2, the orthorhombic phase occurred at 473 K and the area of the orthorhombic phase further increased at 573 K. It was also observed that more trigonal phase transformed into orthorhombic phase under the GSSe-2 coating sequence, where Sb-Se serves as the initial layer in the modulation period.

In contrast to the Ge-Sb-Sn SLL thin films, the characteristic peak around 29° (1 0 1) was absent in most Ge-Sb-Se thin films and the preferential orientation of R-3m space group shifted to (2 1 3), detailed in Supplementary Figure 9. In addition, no significant continuous shift of the R-3m peaks occurred in Ge-Sb-Se thin films, which indicates that the main crystalline trigonal phase remains pure Sb. In comparison, the Ge-Sb-Se ternary system demonstrates greater amorphous stability, with its amorphous region area reaching twice the size of the Ge-Sb-Te ternary system when subjected to heat treatment at 573 K for 1 h[27]. However, the relatively low symmetry of the Pnma space group and the difference in atomic sizes

(Sb: 133 pm, Se: 103 pm) could lead to lower cyclability of Ge-Sb-Se thin films for photonic applications, which requires further investigation.

Optical performance of SLL thin films

Ge-Sb-Sn ternary system

For optical switches and all-optical memories based on phase-change storage materials, their optical loss in the communication bands is an urgent issue to be solved[41]. In the near-infrared, O-band (original band: 1,260-1,360 nm) and C-band (conventional band: 1,530-1,565 nm) are in extensive use for optical communication. The optical loss in the two bands determines the capability of optical transmission in short- and long-distance fiber-optic communication systems, respectively[42]. Figure 4 presents maps of the extinction coefficient (k) of amorphous Ge-Sb-Sn SLL combinatorial thin films in different coating sequences (GSSn-1 and GSSn-2) under wavelengths of 1,310 (O-band) and 1,550 nm (C-band) across the entire compositional range. Optical constants of the wavelengths are taken from the full spectrum fitted by the three-layer model introduced in the Methods section. More details of the fitting results are shown in Supplementary Figures 10 and 11. Under the GSSn-1 sequence, the value of k shows a strong dependency on the composition, decreasing progressively and almost linearly from the Sn-rich corner to the Ge-Sb binary edge. In contrast, under the GSSn-2 sequence, the value of k decreases from the corners toward the center of the map, and the values are lowered by half compared to the GSSn-1 near the Sn-rich corner. This can be explained by the different light-absorbing nature of the SLL thin films in three distinct regions within a single thin film structure: (1) within the bulk of the thin film; (2) at the interface of the thin film and the substrate; (3) at the interface of the thin film and air. Different coating sequences of the SLL thin films change the extent of optical absorbance at the interfaces and, therefore, result in a significant variation in k distribution.

To generally evaluate the optical performance of SLL thin films, the figure of merit (*FOM*) coupling of n and k is adopted. The *FOM* formula can be expressed as:

$$FOM = \frac{|n_{anneal} - n_0|}{k_{anneal} + k_0} \tag{2}$$

where n_{anneal}, n_0 and k_{anneal}, k_0 represent the refractive index and extinction coefficient of the SLL thin films heat-treated at 573 K for 1 h and in the as-deposited state, respectively. Conclusive evidence suggests that this general *FOM* value exhibits a quantitative correlation with the performance of numerous types of photonic devices. Specifically, a higher *FOM* value is indicative of superior optical properties[43]. Materials with a high FOM are particularly valuable for applications such as optical switches, display technologies, and phase-change photonic devices, where maximizing optical contrast while minimizing optical losses is essential. We propose a map distribution of *FOM* for the Ge-Sb-Sn SLL thin films at wavelengths of 1,310 and 1,550 nm (annealed at 573 K for 1 h), shown in Figure 5. Datasets used for the calculation of *FOM* for the Ge-Sb-Sn and Ge-Sb-Se SLL thin films are illustrated in Supplementary Figures 12-17. Based on Figures 2, 4, and 5, SLL thin films with a composition near $GeSbSn_3$ under the GSSn-2 deposition sequence are screened out as a promising candidate for non-volatile photonic memories. This region has a value of *FOM* greater than 0.4 and maintains fairly good amorphous stability at 573 K with the potential for transition to a high-symmetry tetrahedral phase. While the Ge-rich region has better amorphous stability, it greatly suppresses the phase transition process and leads to a larger loss of *FOM*.

Ge-Sb-Se ternary system

Figures 6 and 7 illustrated the maps of k and *FOM* of Ge-Sb-Se SLL combinatorial thin films in different

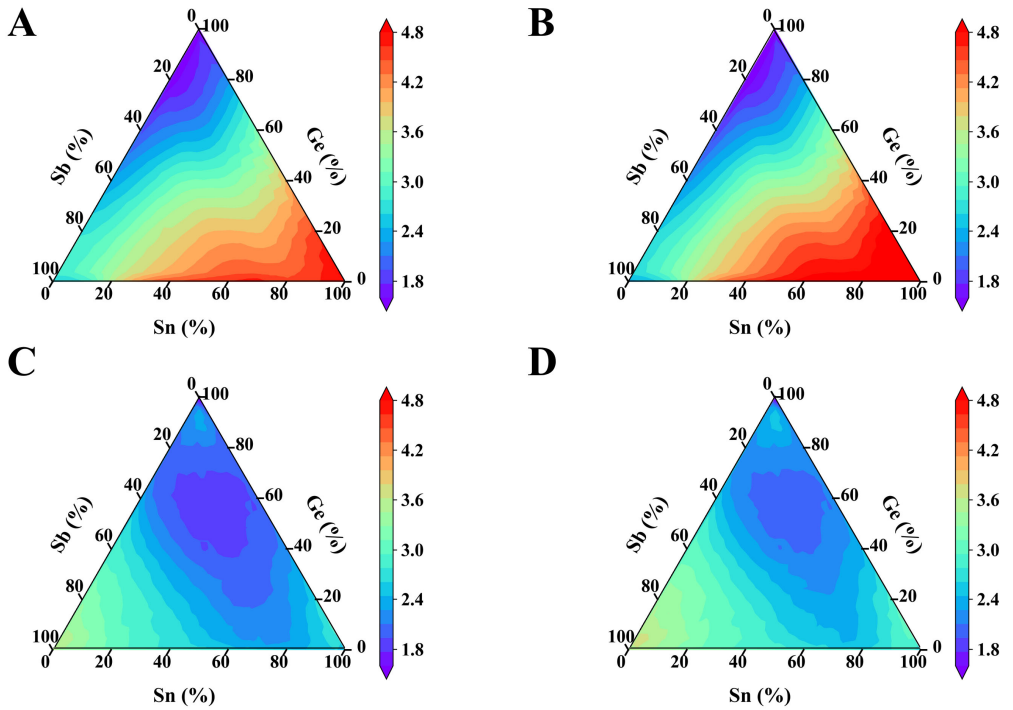

Figure 4. Distribution of extinction coefficient (*k*) as deposited. (A) GSSn-1 at a wavelength of 1,310 nm; (B) GSSn-1 at a wavelength of 1,550 nm; (C) GSSn-2 at a wavelength of 1,310 nm; (D) GSSn-2 at a wavelength of 1,550 nm.

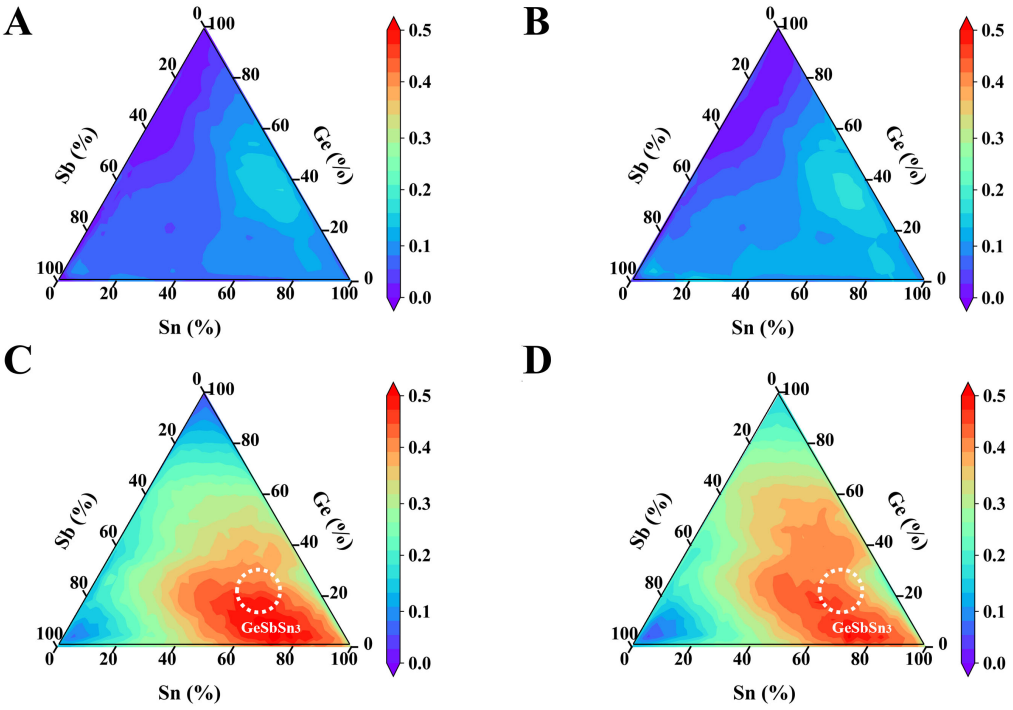

Figure 5. Distribution of FOM (573 K). (A) GSSn-1 at a wavelength of 1,310 nm; (B) GSSn-1 at a wavelength of 1,550 nm; (C) GSSn-2 at a wavelength of 1,310 nm; (D) GSSn-2 at a wavelength of 1,550 nm.

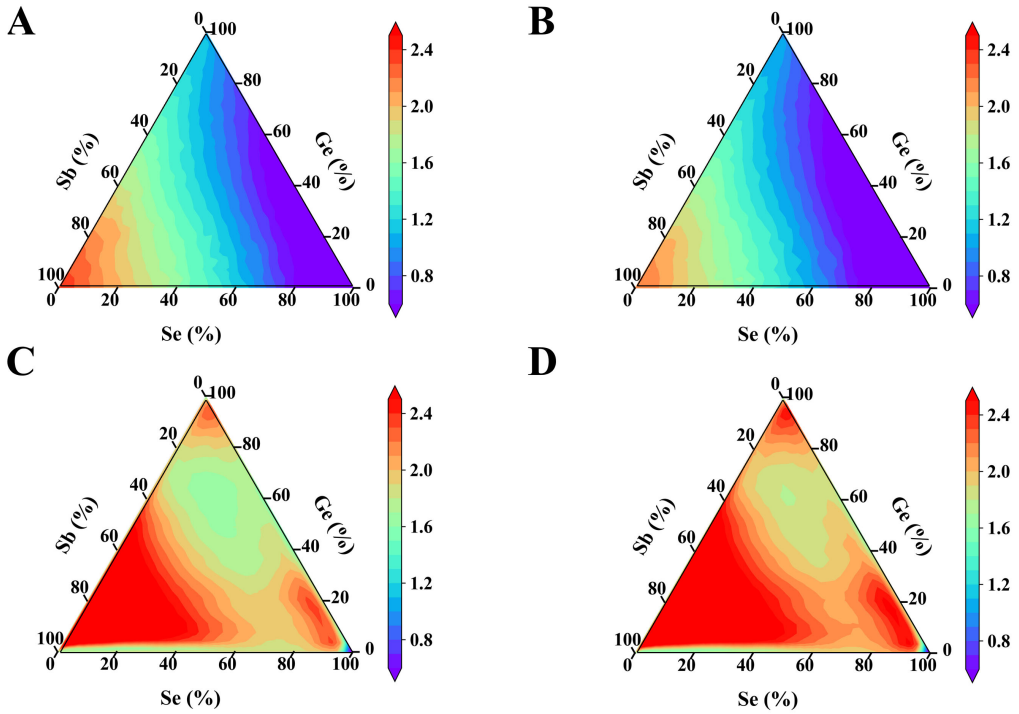

Figure 6. Distribution of extinction coefficient (*k*). (A) GSSe-1 at a wavelength of 1,310 nm; (B) GSSe-1 at a wavelength of 1,550 nm; (C) GSSe-2 at a wavelength of 1,310 nm; (D) GSSe-2 at a wavelength of 1,550 nm.

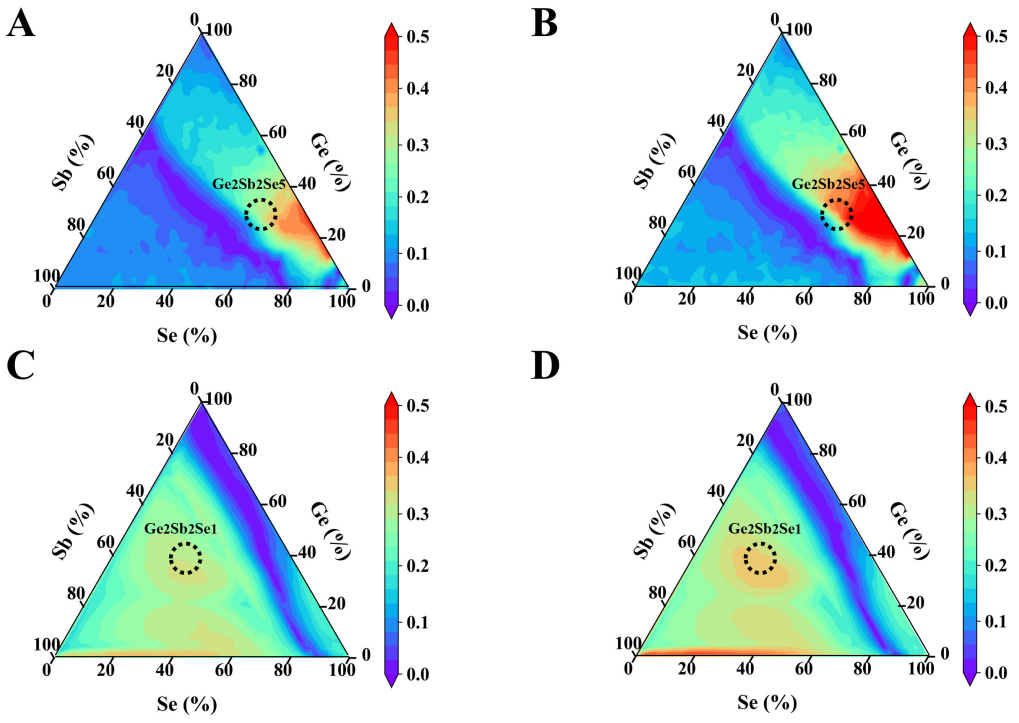

Figure 7. Distribution of FOM (573 K). (A) GSSe-1 at a wavelength of 1,310 nm; (B) GSSe-1 at a wavelength of 1,550 nm; (C) GSSe-2 at a wavelength of 1,310 nm; (D) GSSe-2 at a wavelength of 1,550 nm.

coating sequences (GSSe-1 and GSSe-2) under wavelengths of 1,310 (O-band) and 1,550 nm (C-band), respectively. Notably, the *k* values near the Se-rich corner reach the lowest of the overall distribution for both sequences. As discussed above, based on Figure 3, while the Ge-Sb-Se SLL combinatorial thin films exhibit superior amorphous stability, the relatively low symmetry of the Pnma space group may limit their cyclability for photonic applications. Nevertheless, promising candidates for phase change materials (PCMs) were identified as $Ge_2Sb_2Se_5$ under the GSSe-1 sequence and $Ge_2Sb_2Se_1$ under the GSSe-2 sequence. Both have good transmittance in the amorphous state and FOM values greater than 0.3. Additionally, in the component region around $Ge_2Sb_2Se_5$, a novel PCM alloy $Ge_2Sb_2Se_4Te_1$ has been reported to possess unprecedented broadband transparency over the infrared wavelength range. Our findings provide valuable insights for future research on Ge-Sb-Se-Te quaternary alloys. The boundary effect[27] and a small amount of melting in the Se(Sn)-rich corner (Se-content above 95%, Sn-content above 85%)[44] have been taken into account in our screening analysis.

The Ge-Sb-Sn and Ge-Sb-Se SLL ternary systems exhibit distinct phase evolution behaviors and optical properties. The Ge-Sb-Sn system shows a greater potential for multi-level phase transitions, accompanied by a significant optical contrast between the phases before and after the transition. In contrast, the Ge-Sb-Se system demonstrates superior amorphous stability and lower optical loss in the amorphous state. Both systems provide valuable insights into the development of conventional CPCMs, particularly in addressing the challenges of high energy consumption and inadequate amorphous stability. Furthermore, these systems lay a critical foundation for future investigations of the Ge-Sb-based quaternary system.

CONCLUSIONS

A multi-parameter mapping of composition-structure-process-property relationships in Ge-Sb-Sn/Se combinational SLL thin films has been rapidly constructed via a data-driven high-throughput methodology. Our investigation systematically analyzes the influence of chemical composition, structural characteristics, and synthesis deposition on both phase evolutions and optical properties. Through this analysis, we have identified several promising candidates for non-volatile memory within Ge-Sb-Sn and Ge-Sb-Se SLL thin films that exhibit optimal characteristics of amorphous stability and optical performance. Notably, the $GeSbSn_3$ SLL thin film under the Sb→Sn→Ge deposition sequence has a value of *FOM* exceeding 0.4 with high thermal stability. Structural evolutions from trigonal to hexagonal/tetrahedral have been systematically identified across distinct compositional ranges in the Ge-Sb-Sn combinatorial thin films, demonstrating their potential for enabling multi-level switching functionality. These findings not only establish fundamental guidance for future studies in Ge-Sb-based quaternary system, but also bolster our upcoming efforts to integrate artificial intelligence with high-throughput experimental datasets, facilitating the advancement of all-photonic memory computing based on CPCMs.

DECLARATIONS

Acknowledgments

The authors sincerely thank Yang Ren for his administrative, technical, and material support.

Authors' contributions

Investigation, writing - original draft, visualization, data curation, validation, formal analysis: Yuan, H.
Visualization; data curation: Lu, J.
Conducting experiments: Zhuang, G.
Writing - review & editing; project administration; supervision; funding acquisition: Wang, H.
Writing - review & editing; conceptualization; supervision; funding acquisition; investigation; methodology: Hui, J.

Availability of data and materials

Data supporting our findings can be found in the Supplementary Materials. Other raw data that support the findings of this study are available from the corresponding author upon reasonable request.

Financial support and sponsorship

This research was supported by "Shanghai Jiao Tong University the Initiation Programme for New Teachers" (No. AF0500207), the National Key Research and Development Program of China (Grant No. 2021YFB3702104), the Advanced Materials-National Science and Technology Major Project (Grant No. 2024ZD0608300), and the Zhiyuan Future Scholar Program (Grants No. 2024-23) from Shanghai Jiao Tong University.

Conflicts of interest

All authors declared that there are no conflicts of interest.

Ethical approval and consent to participate

Not applicable.

Consent for publication

Not applicable.

REFERENCES

1. Ríos, C.; Stegmaier, M.; Hosseini, P.; et al. Integrated all-photonic non-volatile multi-level memory. *Nat. Photon.* **2015**, *9*, 725-32. DOI
2. Feldmann, J.; Stegmaier, M.; Gruhler, N.; et al. Calculating with light using a chip-scale all-optical abacus. *Nat. Commun.* **2017**, *8*, 1256. DOI PubMed PMC
3. Liu, B.; Li, K.; Liu, W.; et al. Multi-level phase-change memory with ultralow power consumption and resistance drift. *Sci. Bull.* **2021**, *66*, 2217-24. DOI
4. Wen, S.; Meng, Y.; Jiang, M.; Wang, Y. Multi-level coding-recoding by ultrafast phase transition on $Ge_2Sb_2Te_5$ thin films. *Sci. Rep.* **2018**, *8*, 4979. DOI PubMed PMC
5. Kim, E. T.; Lee, J. Y.; Kim, Y. T. Investigation of the structural transformation behavior of $Ge_2Sb_2Te_5$ thin films using high resolution electron microscopy. *Appl. Phys. Lett.* **2007**, *91*, 101909. DOI
6. Wuttig, M.; Bhaskaran, H.; Taubner, T. Phase-change materials for non-volatile photonic applications. *Nat. Photon.* **2017**, *11*, 465-76. DOI
7. Yue, L.; Fang, T.; Zheng, S.; et al. Cu/Sb codoping for tuning carrier concentration and thermoelectric performance of GeTe-based alloys with ultralow lattice thermal conductivity. *ACS. Appl. Energy. Mater.* **2019**, *2*, 2596-603. DOI
8. Wei, S. J.; Zhu, H. F.; Chen, K.; et al. Phase change behavior in titanium-doped $Ge_2Sb_2Te_5$ films. *Appl. Phys. Lett.* **2011**, *98*, 231910. DOI
9. Yin, Q.; Chen, L. Enhanced optical properties of Sn-doped $Ge_2Sb_2Te_5$ thin film with structural evolution. *J. Alloys. Compd.* **2019**, *770*, 692-700. DOI
10. Vinod, E. M.; Ramesh, K.; Sangunni, K. S. Structural transition and enhanced phase transition properties of Se doped $Ge_2Sb_2Te_5$ alloys. *Sci. Rep.* **2015**, *5*, 8050. DOI PubMed PMC
11. Agati, M.; Renaud, F.; Benoit, D.; Claverie, A. In-situ transmission electron microscopy studies of the crystallization of N-doped Ge-rich GeSbTe materials. *MRS. Commun.* **2018**, *8*, 1145-52. DOI
12. Bourgeois, G.; Meli, V.; Al, M. F.; et al. Carbon ion implantation as healing strategy for improved reliability in phase-change memory arrays. *Microelectron. Reliab.* **2021**, *126*, 114221. DOI
13. Shen, J.; Lv, S.; Chen, X.; et al. Thermal barrier phase change memory. *ACS. Appl. Mater. Interfaces.* **2019**, *11*, 5336-43. DOI
14. Chong, T. C.; Shi, L. P.; Zhao, R.; et al. Phase change random access memory cell with superlattice-like structure. *Appl. Phys. Lett.* **2006**, *88*, 122114. DOI
15. Lee, M. L.; Yong, K. T.; Gan, C. L.; Ting, L. H.; Muhamad, D. S. B.; Shi, L. P. Crystallization and thermal stability of Sn-doped $Ge_2Sb_2Te_5$ phase change material. *J. Phys. D. Appl. Phys.* **2008**, *41*, 215402. DOI
16. Lazarenko, P.; Kovalyuk, V.; An, P.; et al. Low power reconfigurable multilevel nanophotonic devices based on Sn-doped $Ge_2Sb_2Te_5$

thin films. *Acta. Mater.* **2022**, *234*, 117994. DOI

17. Xu, P.; Zheng, J.; Doylend, J. K.; Majumdar, A. Low-loss and broadband nonvolatile phase-change directional coupler switches. *ACS. Photonics.* **2019**, *6*, 553-7. DOI
18. Zhang, H.; Yang, X.; Lu, L.; Chen, J.; Rahman, B. M. A.; Zhou, L. Comparison of the phase change process in a GST-loaded silicon waveguide and MMI. *Opt. Express.* **2021**, *29*, 3503-14. DOI
19. Fang, Z.; Zheng, J.; Saxena, A.; Whitehead, J.; Chen, Y.; Majumdar, A. Non-volatile reconfigurable integrated photonics enabled by broadband low-loss phase change material. *Adv. Opt. Mater.* **2021**, *9*, 2002049. DOI
20. Halenkovič, T.; Baillieul, M.; Gutwirth, J.; Němec, P.; Nazabal, V. Amorphous Ge-Sb-Se-Te chalcogenide films fabrication for potential environmental sensing and nonlinear photonics. *J. Materiomics.* **2022**, *8*, 1009-19. DOI
21. Zhang, Y.; Chou, J. B.; Li, J.; et al. Broadband transparent optical phase change materials for high-performance nonvolatile photonics. *Nat. Commun.* **2019**, *10*, 4279. DOI PubMed PMC
22. Hu, Y.; Feng, X.; Li, S.; et al. Superlattice-like $Sb_{50}Se_{50}/Ga_{30}Sb_{70}$ thin films for high-speed and high density phase change memory application. *Appl. Phys. Lett.* **2013**, *103*, 152107. DOI
23. Hui, J.; Hu, Q.; Luo, Y.; et al. Phase evolution and amorphous stability upon solid-state reaction in superlattice-like Ge-Sb-Te combinatorial thin films. *ACS. Appl. Electron. Mater.* **2020**, *2*, 3880-8. DOI
24. Agati, M.; Gay, C.; Benoit, D.; Claverie, A. Effects of surface oxidation on the crystallization characteristics of Ge-rich Ge-Sb-Te alloys thin films. *Appl. Surf. Sci.* **2020**, *518*, 146227. DOI
25. Xu, J.; Qi, C.; Chen, L.; Zheng, L.; Xie, Q. The microstructural changes of $Ge_2Sb_2Te_5$ thin film during crystallization process. *AIP. Adv.* **2018**, *8*, 055006. DOI
26. Teng, N.; Qin, J.; Chen, Y.; Wang, R.; Shen, X.; Xu, T. Optical properties and thermal stability of amorphous Ge-Sb-Se films. *J. Non. Cryst. Solids.* **2020**, *532*, 119888. DOI
27. Hui, J.; Hu, Q.; Yuan, H.; et al. High-throughput study of amorphous stability and optical properties of superlattice-like Ge-Sb-Te thin films. *Small* **2024**, *20*, e2307792. DOI
28. Hui, J.; Hu, Q.; Zhang, H.; et al. High-throughput investigation of structural evolution upon solid-state in Cu-Cr-Co combinatorial multilayer thin-film. *Mater. Des.* **2022**, *215*, 110455. DOI
29. Donald, E. Pybaselines: a python library of algorithms for the baseline correction of experimental data. *Zenodo* 2022. DOI
30. Virtanen, P.; Gommers, R.; Oliphant, T. E.; et al. SciPy 1.0: fundamental algorithms for scientific computing in Python. *Nat. Methods.* **2020**, *17*, 261-72. DOI
31. Murtagh, F.; Contreras, P. Methods of hierarchical clustering; 2011. Available from: https://arxiv.org/abs/1105.0121 [Last accessed on 11 Mar 2025].
32. Weber, J. W.; Hansen, T. A. R.; van de Sanden, M. C. M.; Engeln, R. B-spline parametrization of the dielectric function applied to spectroscopic ellipsometry on amorphous carbon. *J. Appl. Phys.* **2009**, *106*, 123503. DOI
33. Yamada, N.; Matsunaga, T. Structure of laser-crystallized $Ge_2Sb_{2+x}Te_5$ sputtered thin films for use in optical memory. *J. App. Phys.* **2000**, *88*, 7020-8. DOI
34. Kyono, A.; Hayakawa, A.; Horiki, M. Selenium substitution effect on crystal structure of stibnite (Sb_2S_3). *Phys. Chem. Minerals.* **2015**, *42*, 475-90. DOI
35. Akhtar, D.; Vankar, V.; Goel, T.; Chopra, K. Metastable structures of splat-cooled and vapour-depodited lead and antimony films. *Thin. Solid. Films.* **1979**, *58*, 327-32. DOI
36. Salamat, A.; Briggs, R.; Bouvier, P.; et al. High-pressure structural transformations of Sn up to 138 GPa: angle-dispersive synchrotron x-ray diffraction study. *Phys. Rev. B.* **2013**, *88*, 104104. DOI
37. Wu, S.; Son, B.; Zhang, L.; et al. Effects of high-temperature thermal annealing on GeSn thin-film material and photodetector operating at 2 μm. *J. Alloys. Compd.* **2021**, *872*, 159696. DOI
38. Eising, G.; Niebuur, B.; Pauza, A.; Kooi, B. J. Competing crystal growth in Ge-Sb phase-change films. *Adv. Funct. Mater.* **2014**, *24*, 1687-94. DOI
39. Janicki, T. D.; Wan, Z.; Liu, R.; Evans, P. G.; Schmidt, J. R. Guiding epitaxial crystallization of amorphous solids at the nanoscale: interfaces, stress, and precrystalline order. *J. Chem. Phys.* **2022**, *157*, 100901. DOI
40. Jin, B.; Shao, C.; Wang, Y.; Mu, Z.; Liu, Z.; Tang, R. Anisotropic epitaxial behavior in the amorphous phase-mediated hydroxyapatite crystallization process: a new understanding of orientation control. *J. Phys. Chem. Lett.* **2019**, *10*, 7611-6. DOI
41. Ríos, C.; Du, Q.; Zhang, Y.; et al. Ultra-compact nonvolatile phase shifter based on electrically reprogrammable transparent phase change materials. *PhotoniX* **2022**, *3*, 70. DOI
42. Yurchenko, A. V.; Gorlov, N. I.; Alkina, A. D.; Mekhtiev, A. D.; Kovtun, A. A. Research of the additional losses occurring in optical fiber at its multiple bends in the range waves 1310 nm, 1550 nm and 1625 nm long. *J. Phys. Conf. Ser.* **2016**, *671*, 012001. DOI
43. Sun, X. Y.; Du, Q.; Goto, T.; et al. Single-step deposition of cerium-substituted yttrium iron garnet for monolithic on-chip optical isolation. *ACS. Photonics.* **2015**, *2*, 856-63. DOI
44. Ghosh, G. The sb-se (antimony-selenium) system. *J. Phase. Equilibria.* **1993**, *14*, 753-63. DOI